Hindawi
Advances in Materials Science and Engineering
Volume 2021, Article ID 8085949, 13 pages
https://doi.org/10.1155/2021/8085949

Research Article

Dynamic Compression Behavior and a Damage Constitutive Model of Steel Fibre Reinforced Self-Compacting Concrete

Liang Bian [1], Jian Ma [1,2], Jie Zhang [1], and Ping Li [3]

[1] *School of Naval Architecture and Civil Engineering, Jiangsu University of Science and Technology, Zhangjiagang, Jiangsu 215600, China*
[2] *CAS Key Laboratory of Mechanical Behavior and Design of Materials, Department of Modern Mechanics, University of Science and Technology of China, Hefei, Anhui 230027, China*
[3] *School of Management Science and Engineering, Anhui University of Technology, Maanshan, Anhui 243032, China*

Correspondence should be addressed to Liang Bian; liangbian@just.edu.cn

Received 18 June 2021; Revised 23 October 2021; Accepted 29 October 2021; Published 17 November 2021

Academic Editor: José António Fonseca de Oliveira Correia

The dynamic behavior of steel fibre reinforced self-compacting concrete (SFRSCC) was investigated by using a split Hopkinson pressure bar (SHPB). SFRSCC specimens with two strength classes of about 40 MPa and 60 MPa were prepared. Different steel fibre volume fractions were used varying from 0.5% to 2.0%. The tested strain rate ranged from about 50 to 240 s^{-1}. Significant rate dependence was observed, and dynamic increase factor (DIF) was used to quantify the rate sensitivity. The results showed that both the matrix strength and fibre content had effect on the strain rate sensitivity of SFRSCC. A DIF formula was proposed for describing the dynamic strength of SFRSCC at high strain rates, and a dynamic damage constitutive model was derived to describe the stress-strain relationship of SFRSCC. The parameters in the model were determined by fitting the experimental data. Good consistency between theoretical curves and experimental data was obtained.

1. Introduction

Concrete structures may be exposed to impact loading conditions during their functional life, such as moving vehicles impacts, violent earthquakes, bomb blasts, and missile attacks [1–3]. However, plain concrete exhibits insufficient capacity to resist impact loads due to its low tensile strength and poor resistance to cracking. Adding fibres can improve the energy absorption capacity of the matrix and enhancing the mechanical properties and ductility of concrete [4–6]. Among the fibres, the most commonly used are the steel fibres which provide reinforcement by bridging the cracks in concrete under various loads. It was also found that concrete reinforced with steel fibres showed better impact resistance than other fibres such as polypropylene (PP) fibres or polyethylene (PE) fibres [7, 8]. Steel fibre reinforced concrete is being widely used in civil and military structural applications including road pavements, bridges, channel lining, offshore structures, and military infrastructures [9, 10].

Although fibre reinforced concrete has its advantages in improving the impact resistance, it must be noted that the addition of fibres will reduce the workability of concrete and increase the difficulty in vibration work [11, 12]. In addition, the decrease of workability may adversely affect the uniformity of fibre distribution in concrete, which may cause a detrimental effect on the mechanical performance of fibre reinforced concrete [13]. One of the feasible solutions would be using self-compacting concrete (SCC) to enhance the fluidity of the matrix. SCC is a special concrete mixture which can consolidate under its own weight without extra vibration [14]. The mix of steel fibres and SCC is commonly referred to as steel fibre reinforced self-compacting concrete (SFRSCC).

There have been conducted a number of studies on the static behavior of SFRSCC [15–18]. The mechanical properties of SFRSCC are influenced by a great number of parameters including the content and type of cement, aggregate content and size, properties (shape, length, and diameter) of steel fibres, and volume fraction of steel fibres [19–21]. There are still some disagreements in understanding of mechanical properties of SFRSCC. It is difficult to compare the results obtained by different researchers because of the different adopted mix-design and test procedures [22]. In case of advanced design using computer programs, it is necessary to know exact mechanical properties. Thus, a procedure for identifying mechanical and fracture properties of SFRSCC by inverse analysis was presented in [23].

It has been shown that concrete properties such as compressive strength and tensile strength are rate dependent [24–26]. Therefore, the mechanical properties at quasi-static state cannot be applied to structures when dynamic effects are significant [27]. Characterization of these properties under dynamic loading conditions is a necessity. Compared with the quasi-static tests, the dynamic tests are more difficult to conduct, and many additional conditions have to be considered to obtain the real response of SFRSCC to high strain rates [28]. The main devices used to imitate the different strain rates are drop hammer machines and the split Hopkinson pressure bar (SHPB). Kantar et al. [29] presented a study on the impact dynamics of SFRSCC mixes with different fibre contents using a drop-weight testing apparatus. It was found that the impact resistances and the energy dissipation capacities of the SFRSCC plates can be significantly higher than that of pure SCC plates by 6–14 times. Ruiz et al. [27] studied the dynamic mixed-mode fracture of SFRSCC using three-point bending tests. Results showed that the peak load increased with the increase of loading velocity and fibre content. Abid et al. [30] conducted an experimental work to evaluate the performance of SFRSCC under repeated impact loading. The inclusion of micro-steel fibre was found to increase the impact resistance ranging from 150 to 860% compared to plain samples. Li et al. [31] investigated the dynamic properties of self-compacting concrete with 0.5%, 0.75%, and 1.0% steel fibres using a split Hopkinson pressure bar. Results showed that the impact properties including failure modes, peak stress, peak strain, and elastic modulus were all significantly influenced by strain rate and steel fibre content. Steel fibre reinforced SCC showed a more remarkable strain rate effect than that of steel fibre reinforced normal concrete.

It can be seen that the dynamic mechanical properties of SFRSCC are more complex than those under static conditions, and there are few studies on the dynamic damage constitutive model of SFRSCC. It is well known that the failure mechanism of brittle material is complicated since flaws such as cracks and voids commonly exist within the material. These discontinuities have significant effects on the damage evolution and failure characteristics of SFRSCC. It is crucial to develop a model that can describe the damage evolution of SFRSCC under dynamic loading for theoretical and numerical analysis. Burlion et al.[32] assumed that the microvoid evolution is controlled by the plastic volumetric strain, and they proposed a compression damage model for concrete. Johnson et al. [33] also proposed a damage model described by equivalent plastic strain and plastic volumetric strain of concrete. Although the simulation results using the above models were in good agreement with the experiments in some impact problems, these empirical damage models did not give an appropriate definition of damage from the microscopic point of view.

In this study, two strength classes of SFRSCC (40 MPa and 60 MPa) were designed. Dynamic compression tests were carried out to investigate the influence of loading rate, matrix strength, and fibre content on the dynamic mechanical properties of SFRSCC. A dynamic damage constitutive model of SFRSCC was proposed based on the equivalent microvoid hypothesis [34], and the relevant parameters in the model were determined by fitting the experimental data.

2. Materials and Methods

2.1. Mix Proportions. Two types of self-compacting concrete mixtures, with static uniaxial compressive strengths of about 40 MPa and 60 MPa, were designed. Four quantities of steel fibres, 0.5%, 1.0%, 1.5%, and 2.0% in volume ratio, were added to each type of SCC mixture. MC-FX and HC-FX are used for coding for the different mixtures. MC-FX stands for medium strength (40 MPa) SCC, and X is the steel fibre volume fraction in percent. HC-FX stands for high strength (60 MPa) SCC with the steel fibre volume fraction of X percent. The material composition and mix proportions are given in Table 1. The steel fibres, coarse granite aggregate with a maximum size of 16 mm, and natural sand with average fineness modulus of 2.39 are shown in Figure 1. The diameter and length of the steel fibres are 0.2 mm and 10 mm, respectively, the yield strength of the steel fibres is 780 MPa, and the tensile strength is 2800 MPa.

2.2. Mechanical and Rheological Properties. The fluidity and rheology of the fresh SFRSCC mixtures were evaluated by slump flow and L-box tests following the EFNARC guidelines [35]. The measured values for d_m, the largest diameter of the circular spread for concrete to stop flowing (Figure 2), and the ratio of the concrete height of the horizontal and vertical sections in L-box are listed in Table 2.

As for slump flow, all types of SFRSCC exhibited satisfactory results in the range of 710–845 mm, demonstrating acceptable filling ability for practical applications. In L-box tests, the values were also in a practically acceptable range: 0.89–0.94. During the tests, no indication of segregation was observed, and the mixtures maintained good homogeneity and cohesion.

The quasi-static compression tests of SFRSCC were carried out on a hydraulic testing machine with a load capacity of 2000 kN. The specimens were 150 mm cubes at the age of 28 days. Brazilian disc tests were also conducted to obtain the split tensile strength using cylindrical specimens of dimension 70 mm × 35 mm (diameter × height). The basic mechanical properties of SFRSCC are listed in Table 3. The quasi-static compressive strength of SFRSCC for the same type of mixture did not increase with the increase of fibres. Proper amount of steel fibre provides reinforcement for concrete. Higher fibers concentrations, however, may destroy the uniformity of concrete and cause a decrease of the

Table 1: Mix proportions of SFRSCC (kg/m^3).

Mix	Cement	Sand	Coarse aggregate	Fly ash	Water	Superplasticizer	Steel fibres
MC-F0.5	427	724	862	107	171	2.6	39
MC-F1.0	427	721	856	107	171	2.6	78
MC-F1.5	427	714	849	107	171	2.6	117
MC-F2.0	427	708	843	107	171	2.0	156
HC-F0.5	494	714	831	49	148	3.3	39
HC-F1.0	494	696	810	49	148	4.4	78
HC-F1.5	494	678	789	49	148	5.1	117
HC-F2.0	494	658	778	49	148	3.6	156

(a) (b) (c)

Figure 1: Materials used in this study: (a) steel fibres; (b) coarse aggregate; (c) sand.

Figure 2: Slump flow of fresh SFRSCC.

Table 2: Workability of SFRSCC.

Mix	Slump flow d_m (mm)*	L-box h_2/h_1#
MC-F0.5	795	0.91
MC-F1.0	845	0.91
MC-F1.5	750	0.93
MC-F2.0	710	0.90
HC-F0.5	755	0.89
HC-F1.0	750	0.93
HC-F1.5	760	0.93
HC-F2.0	765	0.94

*slump flow values for proper SCC should be within 550–850 mm [35]; #h_2/h_1 values for proper SCC should be ≥0.8 [35].

compressive strength. As still more steel fibers are included, the reinforcement effect provides a gradual increase of the strength [18].

2.3. Dynamic Compression Tests. A 74 mm diameter split Hopkinson pressure bar (SHPB) [36] was used to conduct dynamic compression tests at strain rates between 50 and 240 s^{-1}. The diameter of the specimen is 70 mm and the length is 35 mm. SHPB device consists of a gas gun, a 500 mm long striker bar, a 5.46 m long incident bar, a 3.48 m long transmission bar, and a buffer bar, all made of steel. The photo and schematic diagram of the device are shown in Figure 3. Brass discs placed at the end of the incident bar were used to improve the incident pulse. The rising time of loading pulse then can be increased to meet the requirement of stress uniformity. Also, the high frequency noise in the incident pulse can be reduced.

During the test, the striker launched by the gas gun impacted on the incident bar and generated a compressive pulse propagating in the bar. Due to the mismatching of wave impedances between the specimen and the incident/transmission bars, part of the incident pulse was reflected back to the incident bar, while the rest of the pulse was transmitted through the specimen to the transmission bar. The incident pulse and reflected pulse were recorded by two diametrically opposed strain gauges mounted on the incident bar, and the transmitted pulse was measured by another pair of strain gauges on the transmission bar. The typical incident, reflected, and transmitted pulses recorded in the tests are shown in Figure 4.

According to the measured incident strain ε_i, reflected strain ε_r, and transmitted strain ε_t, the engineering stress σ, engineering strain ε, and engineering strain ε rate experienced by the specimen can be derived by the following equations [36]:

Table 3: Mechanical properties of SFRSCC (standard deviation in parentheses).

Mix	Density (g/cm^3)	Elastic modulus (GPa)	Compressive strength (MPa)	Splitting tensile strength (MPa)
MC-F0.5	2.22 (0.01)	35.6 (2.3)	49.8 (1.1)	3.78 (0.25)
MC-F1.0	2.27 (0.01)	35.0 (1.7)	43.8 (1.9)	4.08 (0.15)
MC-F1.5	2.37 (0.03)	34.9 (1.1)	46.6 (0.9)	4.34 (0.11)
MC-F2.0	2.41 (0.02)	33.4 (1.5)	48.8 (1.8)	5.14 (0.65)
HC-F0.5	2.38 (0.01)	36.6 (1.1)	60.1 (0.3)	4.73 (0.10)
HC-F1.0	2.39 (0.03)	38.0 (1.3)	69.6 (1.4)	5.37 (0.24)
HC-F1.5	2.41 (0.02)	37.7 (2.1)	64.9 (1.0)	4.93 (0.18)
HC-F2.0	2.42 (0.01)	36.3 (1.3)	66.1 (0.4)	5.40 (0.40)

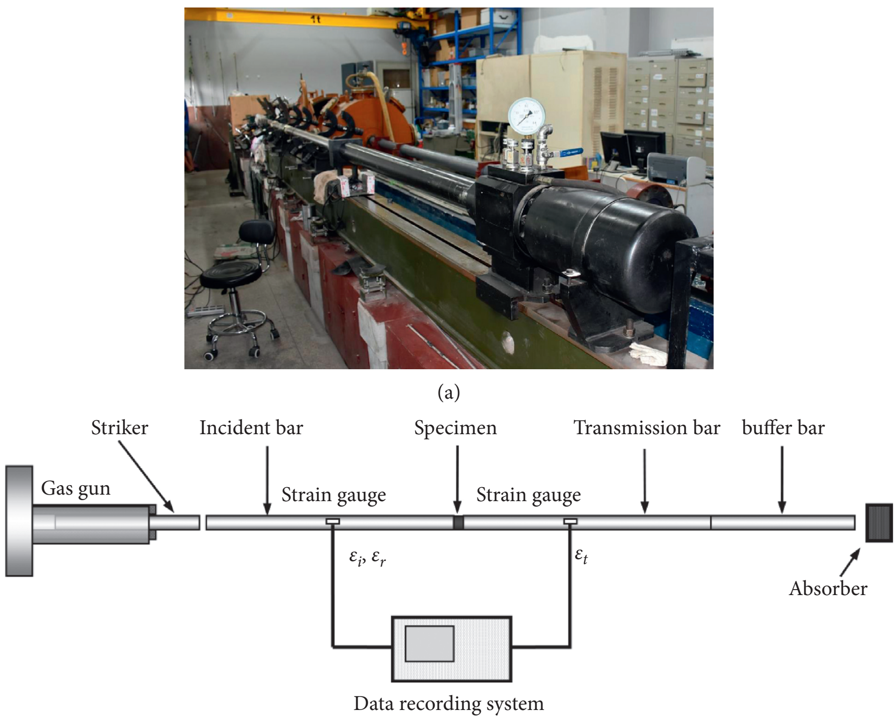

Figure 3: The SHPB setup: (a) photo of the device; (b) schematic diagram of the device.

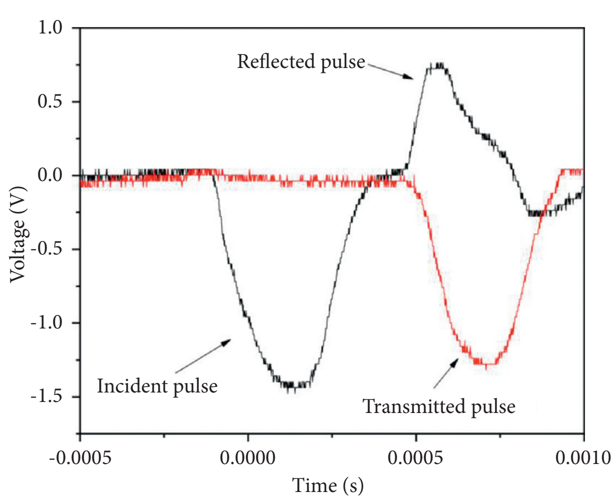

Figure 4: Recorded waveforms from dynamic compression test.

$$\begin{cases} \varepsilon(t) = \dfrac{c_0}{L}\displaystyle\int_0^t [\varepsilon_i(t) - \varepsilon_r(t) - \varepsilon_t(t)]\mathrm{d}t, \\ \dot{\varepsilon}(t) = \dfrac{c_0}{L}[\varepsilon_i(t) - \varepsilon_r(t) - \varepsilon_t(t)], \\ \sigma(t) = \dfrac{EA}{2A_s}[\varepsilon_i(t) + \varepsilon_r(t) + \varepsilon_t(t)], \end{cases} \tag{1}$$

where E is the Young's modulus of the bar, A is the cross-sectional area of the incident/transmission bars, A_s is the cross-sectional area of the specimen, c_0 is the longitudinal wave velocity in the bars, and L is the length of the specimen. If stress equilibrium is satisfied in the specimen, the following expression can be obtained:

$$\varepsilon_i(t) + \varepsilon_r(t) = \varepsilon_t(t). \tag{2}$$

Substituting equation (2) into equation (1) yields

$$\begin{cases} \varepsilon(t) = \dfrac{2c_0}{L}\displaystyle\int_0^t [\varepsilon_i(t) - \varepsilon_t(t)]\mathrm{d}t, \\ \dot{\varepsilon}(t) = \dfrac{2c_0}{L}[\varepsilon_i(t) - \varepsilon_t(t)], \\ \sigma(t) = \dfrac{EA}{A_s}\varepsilon_t(t). \end{cases} \tag{3}$$

Due to the large diameter of the bar, the reflected wave dispersion is usually serious. Therefore, equation (3) is often used to obtain the stress-strain curve for test specimen.

For SFRSCC specimens, the strain rate recorded in the SHPB test varies with time. Three different methods have been used to calculate the strain rate [37]: mean strain rate over the loading period, mean strain rate over a defined stress interval, and strain rate at failure point. In this paper, calculating the strain rate over a defined period was adopted. The range includes the strain rates from the one specified to 40% of the maximum stress to the strain rate corresponding to the maximum stress, as shown in Figure 5.

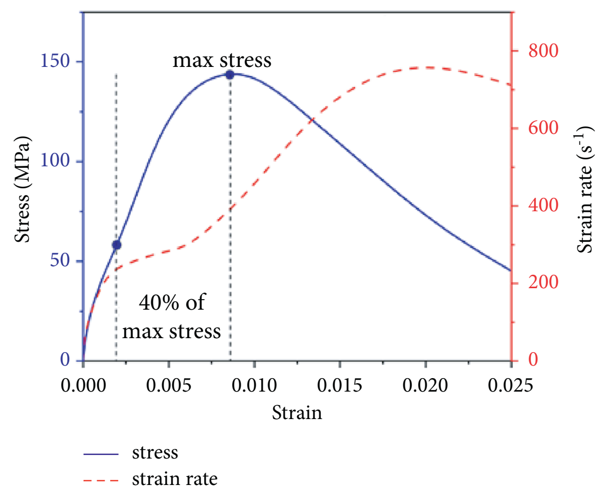

Figure 5: Determination of the strain rate in the specimen.

3. Results and Discussion

3.1. Dynamic Stress-Strain Relationship and Rate Dependence of SFRSCC. The dynamic compressive stress-strain curves obtained in the SHPB tests are presented in Figures 6 and 7 for medium strength and high strength SFRSCC, respectively. Significant rate dependence was observed for all types of SFRSCC. The compressive strength increased with strain rate, and the dynamic strength was much higher than the static value. The maximum peak stress achieved in the tests was up to 220 MPa for HC-F1.5, which was more than three times the static strength (64.9 MPa).

Dynamic increase factor (DIF) is usually used to evaluate the dynamic enhancement effect of concrete strength. DIF is defined as the ratio of dynamic strength to quasi-static strength of concrete. For dynamic compression, DIF $= f_{c,d}/f_{c,s}$, where $f_{c,d}$ is the compressive strength under dynamic loading and $f_{c,s}$ is the quasi-static compressive strength of concrete. So far, many empirical formulas have been proposed to describe the relationship between DIF and strain rate of normal concrete, such as CEB-FIP equation [38]:

$$\mathrm{DIF} = \begin{cases} \left(\dfrac{\dot{\varepsilon}}{\dot{\varepsilon}_0}\right)^{0.014}, & \dot{\varepsilon} \le 30\,\mathrm{s}^{-1}, \\ 0.012\left(\dfrac{\dot{\varepsilon}}{\dot{\varepsilon}_0}\right)^{1/3}, & \dot{\varepsilon} > 30\,\mathrm{s}^{-1}, \end{cases} \tag{4}$$

where $\dot{\varepsilon}_0 = 30 \times 10^{-6}\,\mathrm{s}^{-1}$ is the reference strain rate. Figures 8 and 9 show the variation of DIF with strain rate for medium strength and high strength SFRSCC. The curve defined by the empirical formula CEB-FIP [38] for normal concrete was also plotted for comparison. The experimental data of DIF for medium strength SFRSCC were all located above the CEB-FIP curve within the strain rate range of 53 s^{-1}–184 s^{-1}, as shown in Figure 8, indicating that the strain rate sensitivity of medium strength SFRSCC was higher than normal concrete. The DIF increased with increasing fibre content as well as increasing strain rate.

For high strength SFRSCC, the DIF values were close to the CEB-FIP curve in the strain rate range of 50 s^{-1}–240 s^{-1}, as shown in Figure 9, and the strain rate sensitivity was lower than that of medium strength SFRSCC. The DIF values also increased with the increase of strain rate, but the strain rate sensitivity tended to decrease when the fibre content was more than 1.5%.

An empirical formula was proposed to describe the strain rate sensitivity of the SFRSCC. It assumed a linear increase in DIF with the logarithm of the strain rate:

$$\mathrm{DIF} = A \cdot \log_{10}\left(\frac{\dot{\varepsilon}}{\dot{\varepsilon}_0}\right) + B, \tag{5}$$

where $\dot{\varepsilon}_0 = 30 \times 10^{-6}\,\mathrm{s}^{-1}$ and A and B are constants. A linear regression was carried out to obtain the values of A and B. The results are listed in Table 4. It was found that the slope of

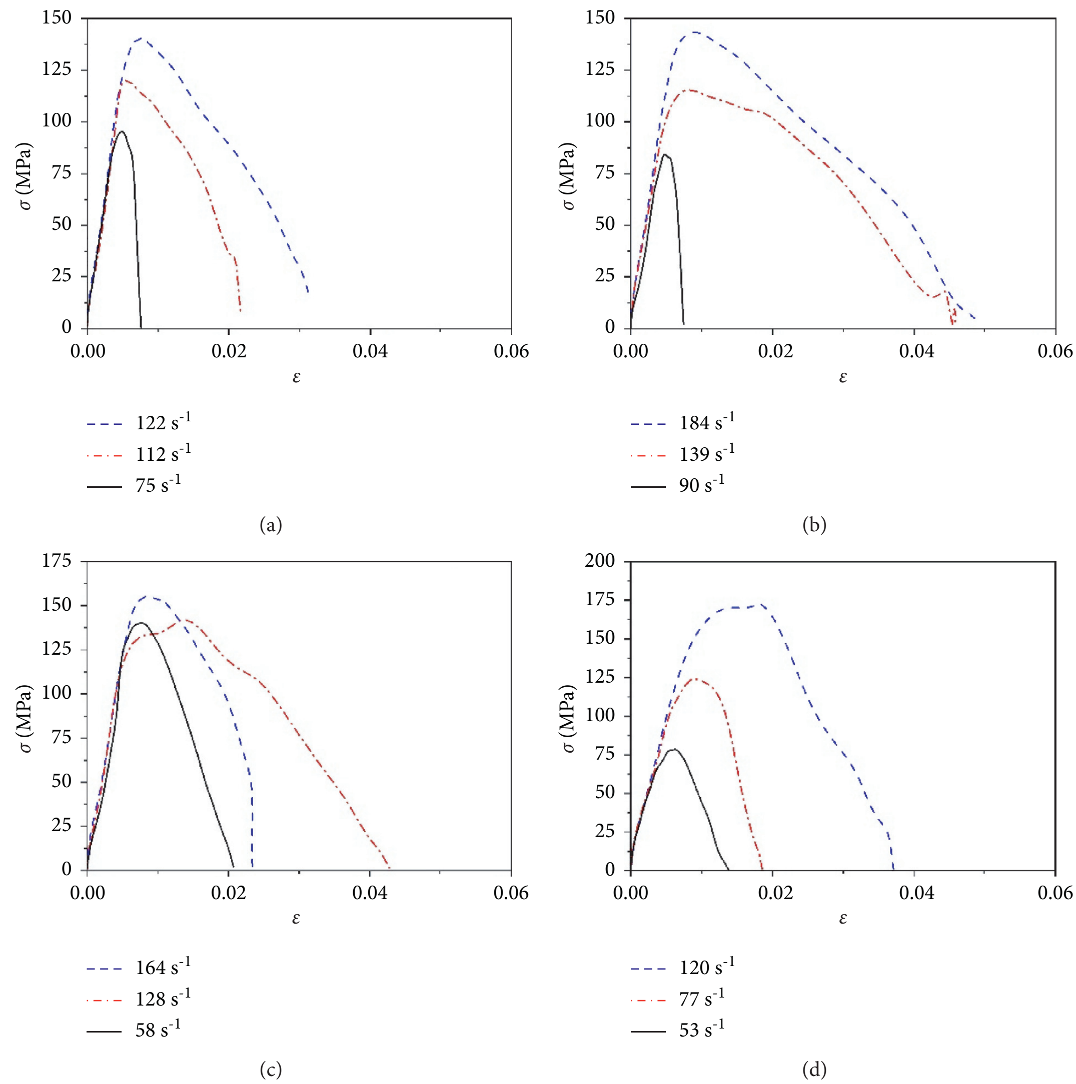

FIGURE 6: Dynamic compressive stress-strain curves of medium strength SFRSCC: (a) MC-F0.5; (b) MC-F1.0; (c) MC-F1.5; (d) MC-F2.0.

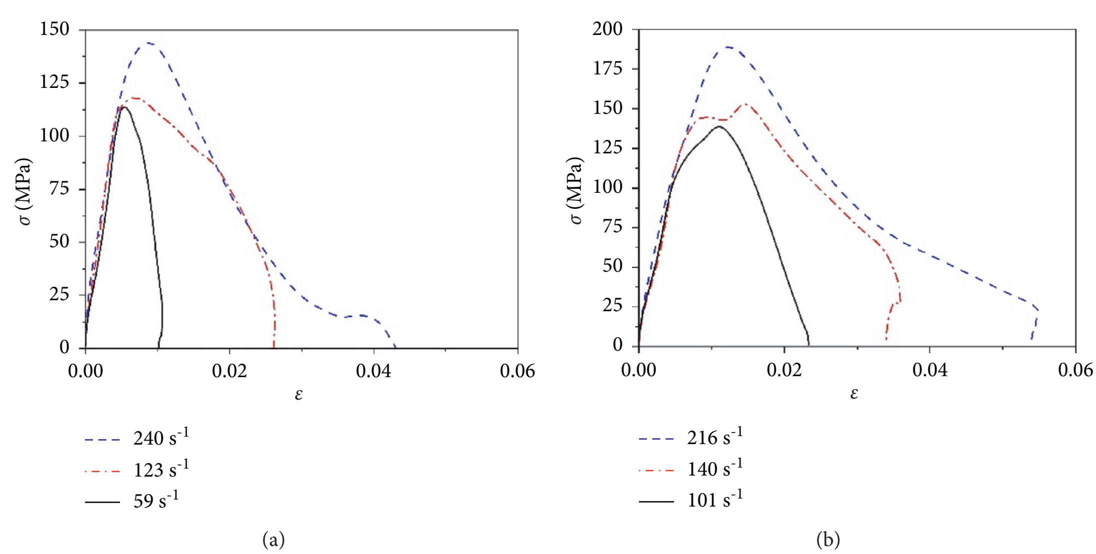

FIGURE 7: Continued.

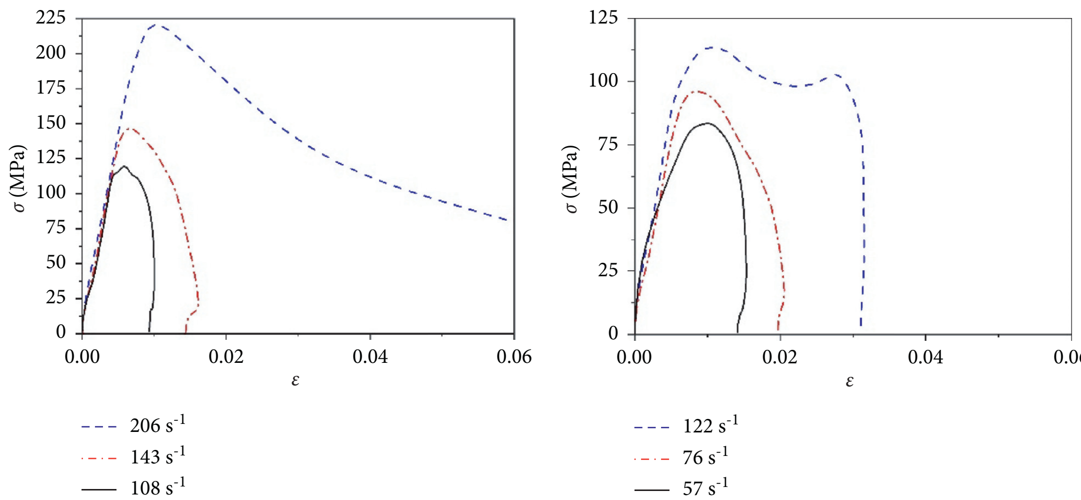

(c) (d)

FIGURE 7: Dynamic compressive stress-strain curves of high strength SFRSCC: (a) HC-F0.5; (b) HC-F1.0; (c) HC-F1.5; (d) HC-F2.0.

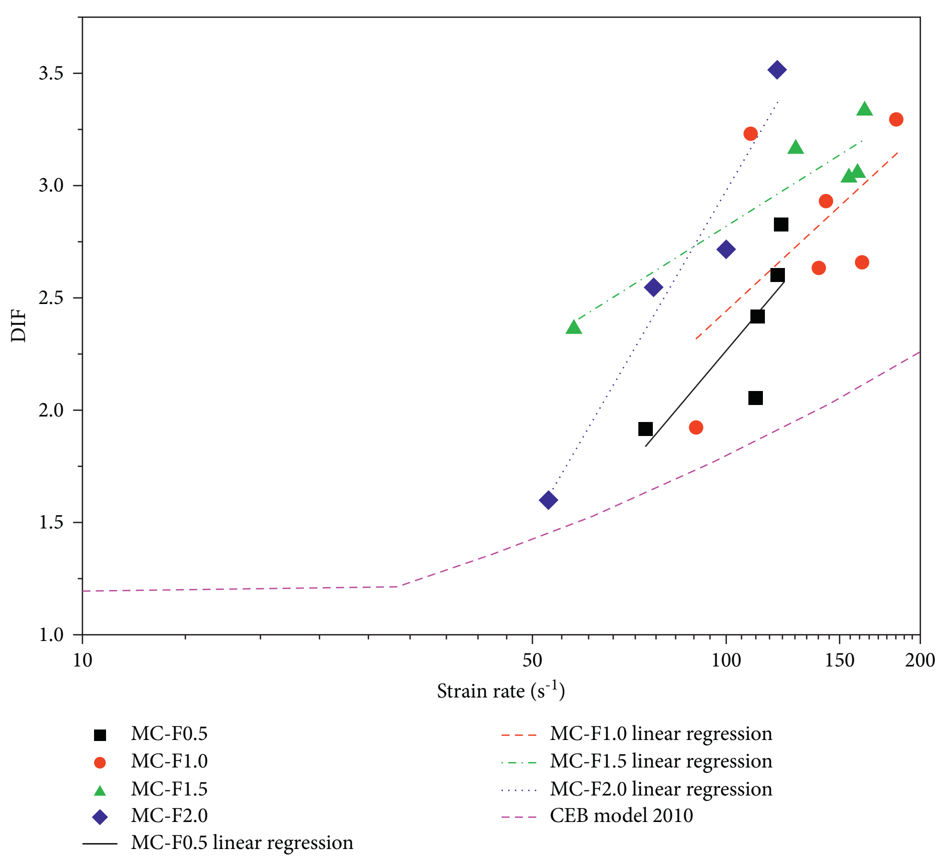

FIGURE 8: Dynamic increase factor for medium strength SFRSCC.

the DIF for medium strength SFRSCC decreased when the fibre content increased from 0.5% to 1.5%, but increased when the fibre content increased from 1.5% to 2.0%. The slope of the DIF for high strength SFRSCC increased when the fibre content increased from 0.5% to 1.5%, but decreased when the fibre content increased from 1.5% to 2.0%.

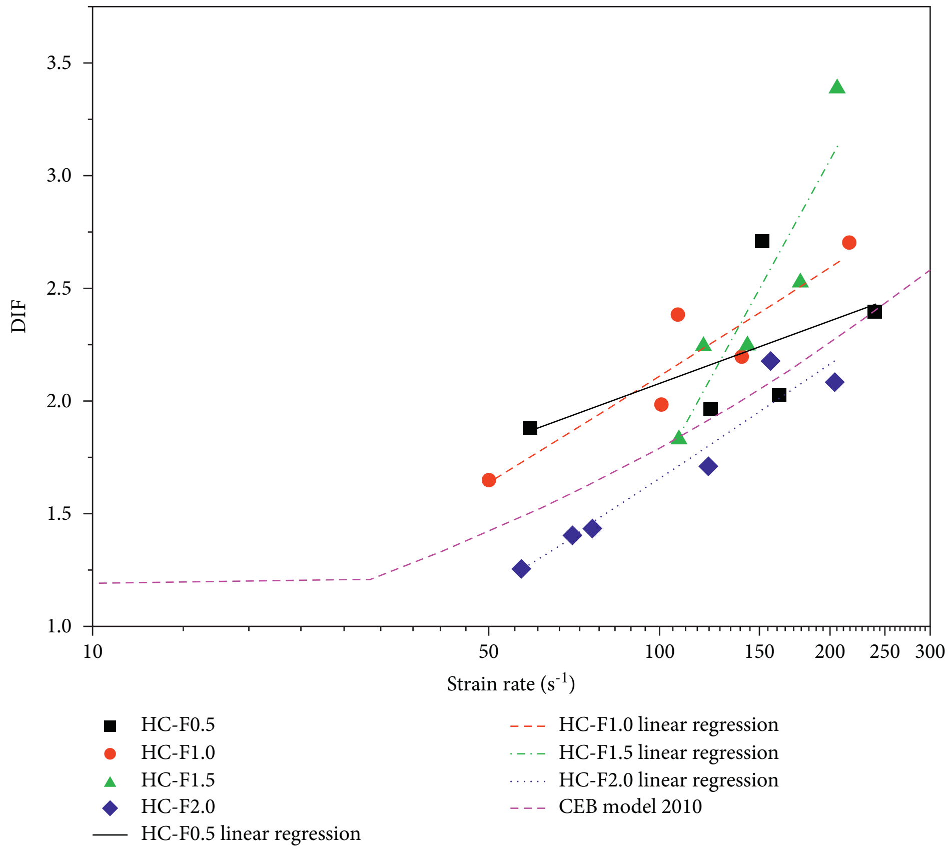

Figure 9: Dynamic increase factor for high strength SFRSCC.

Table 4: Constants in proposed DIF formula for SFRSCC.

Mix	A	B
MC-F0.5	3.4126	−19.9991
MC-F1.0	2.6310	−14.7267
MC-F1.5	1.7937	−8.8893
MC-F2.0	4.9260	−29.1629
HC-F0.5	0.9176	−3.9057
HC-F1.0	1.5821	−8.2046
HC-F1.5	4.5814	−28.1943
HC-F2.0	1.6821	−9.3132

3.2. Influence of the Matrix Strength and Fibre Content on the Behavior of SFRSCC. The experimental results showed that strain rate sensitivity of SFRSCC was affected by both the matrix strength and fibre content. From the microscopic point of view, the main failure mode of SFRSCC during compression is caused by the collapse of microvoids. For low strength SFRSCC, the structural effect is more significant due to high porosity, which makes the material more sensitive to strain rate. The influence of fibres on the DIF may be considered as the additional voids caused by fibres. Generally speaking, increasing of fibres leads to decrease of SFRSCC workability, which implies reduction in compaction levels of SFRSCC. However, in this study, the mix proportions of SFRSCC were optimized in order to satisfy the requirement of strength grade. The workability of SFRSCC did not decrease with the increase of fibre content. As can be seen from Table 2, high strength SFRSCC with 2% fibres showed good fluidity, which result in low sensitive to strain rate.

3.3. Damage Constitutive Model of SFRSCC. Design and nonlinear analysis of structures taking into account the actual behavior of SFRSCC is typically based on the constitutive models [23]. In the present study, a damage constitutive model was developed based on the stress-strain relationship, as demonstrated in Figures 6 and 7. SFRSCC is a heterogeneous material which contains many flaws such as cracks and voids. These cracks and voids grow and develop under external loading, resulting in damage of material. To simplify the analysis, each microvoid and microcrack can be regarded as a spherical cavity with its maximum diameter. The total volume of material can be written as the sum of the total volume of all equivalent microvoids V_d and the total volume of solid parts V_s, i.e., $V = V_s + V_d$. $V_d = \sum v_d(i)$, where $v_d(i)$ represents the volume of the ith equivalent microvoid. The damage of SFRSCC then can be defined as [34]

$$D = \frac{V_d}{V}. \tag{6}$$

Thus,

$$\dot{V}_d = \dot{D}V + \dot{V}D, \tag{7}$$

Table 5: Material parameters in the damage model.

Mix	a (MPa^{-1})	γ
MC-F0.5	5.87×10^5	2.62
MC-F1.0	2.22×10^4	1.94
MC-F1.5	1.04×10^1	0.41
MC-F2.0	5.13×10^4	2.16
HC-F0.5	3.13×10^1	0.52
HC-F1.0	1.06×10^2	0.84
HC-F1.5	2.45×10^5	2.38
HC-F2.0	3.05×10^2	1.20

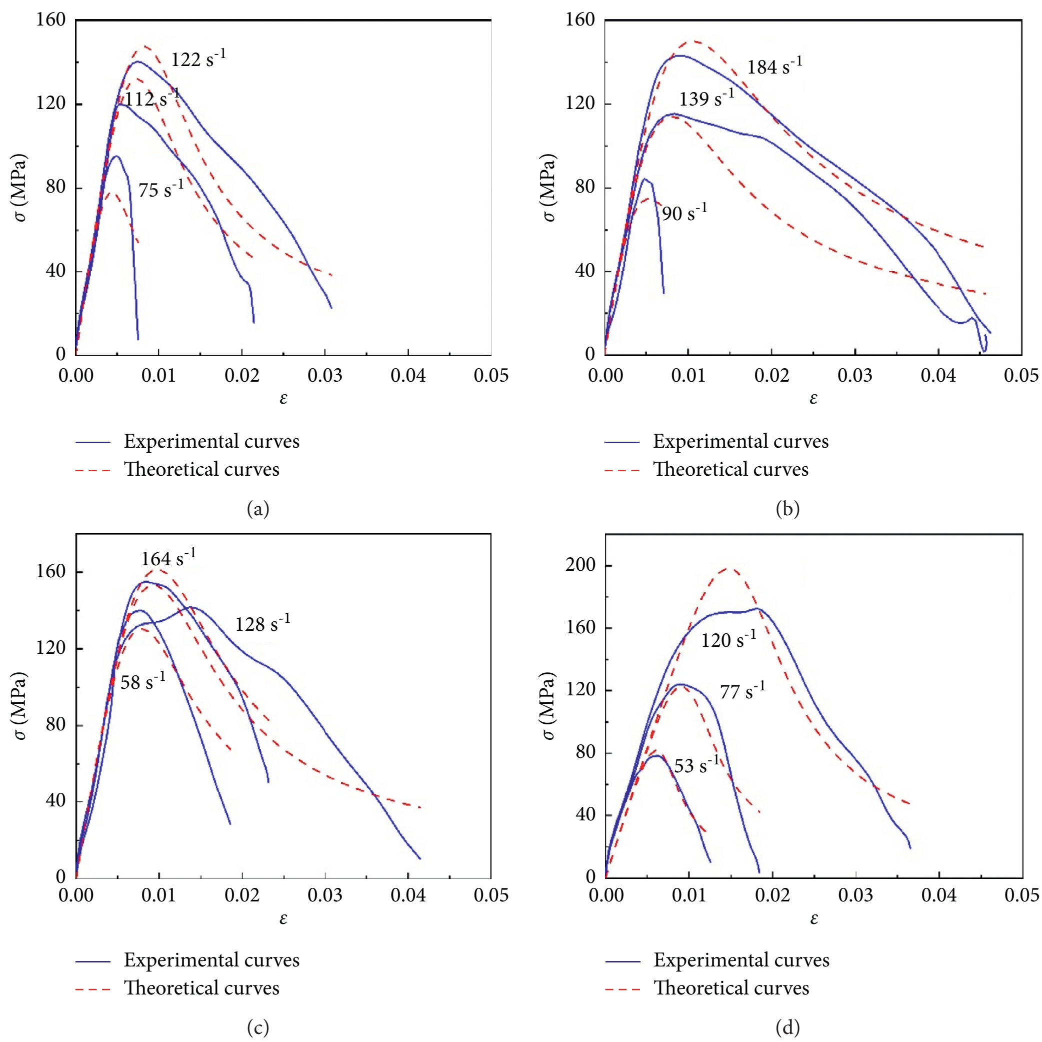

Figure 10: Continued.

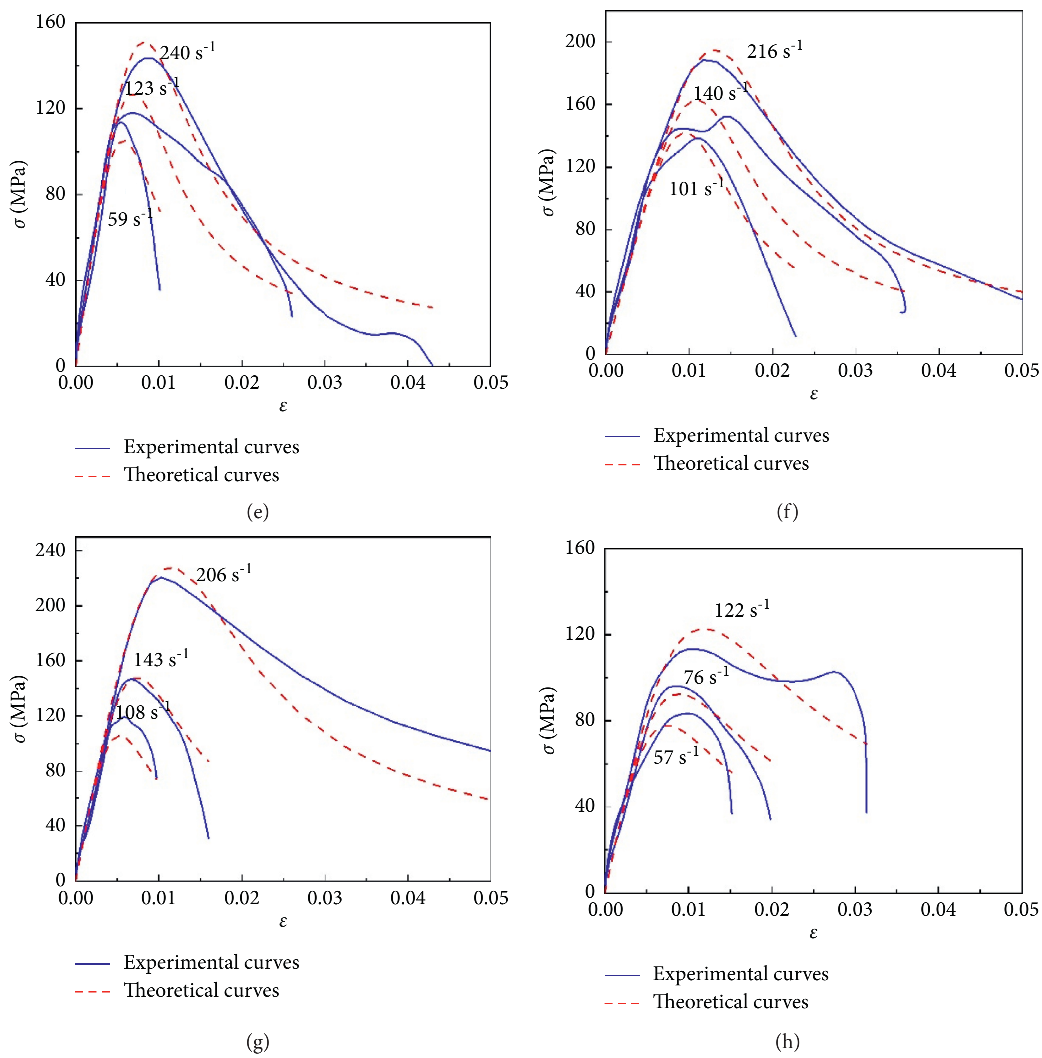

FIGURE 10: Comparison between experimental and theoretical stress-strain curves: (a) MC-F0.5; (b) MC-F1.0; (c) MC-F1.5; (d) MC-F2.0; (e) HC-F0.5; (f) HC-F1.0; (g) HC-F1.5; (h) HC-F2.0.

where the black dot above the variable represents the derivative of time, i.e., $\dot{V}_d = \mathrm{d}V_d/\mathrm{d}t$. If the damage is assumed to develop with the material deformation due to compression and shearing, the relative growth rate of each microvoid can be assumed to be proportional to the rate of work [34]:

$$\frac{\dot{v}_d(i)}{v_d(i)} = \frac{a_1 \dot{W}}{W_B}, \tag{8}$$

where a_1 is the material constant, $\dot{W}$ is the rate of work, and W_B is the normalization factor. Thus, for the whole material, we have

$$\frac{\dot{V}_d}{V_d} = \frac{a_1 \dot{W}}{W_B}. \tag{9}$$

By substituting equation (7) into equation (9) and using equation (6), the damage evolution equation can be obtained as follows:

$$\dot{D} = \frac{a_1 D \dot{W}}{W_B} - D\frac{\dot{V}}{V}. \tag{10}$$

If the solid material is assumed to be incompressible, i.e., $\dot{V}_s = 0$, then

$$\begin{aligned} 0 &= \dot{V}_s \\ &= \dot{V} - \dot{V}_d \\ &= \dot{V} - D\dot{V} - \dot{D}V, \end{aligned} \tag{11}$$

$$\text{or } D\frac{\dot{V}}{V} = \frac{D\dot{D}}{1-D}. \tag{12}$$

Substitution of equation (12) into equation (10) yields

$$\dot{D} = \frac{a_1 D(1-D)\dot{W}}{W_B}. \tag{13}$$

For uniaxial compression,

$$\dot{D} = \frac{a_1 D(1-D)\sigma\dot{\varepsilon}}{W_B}, \tag{14}$$

where σ is the stress and $\dot{\varepsilon}$ is the strain rate. For high strain rates, we assume that W_B is a power function of strain rate:

$$W_B = b_1\left(\frac{\dot{\varepsilon}}{\dot{\varepsilon}_0}\right)^{\gamma}, \tag{15}$$

where b_1 and γ are material constants and $\dot{\varepsilon}_0 = 1\,\mathrm{s}^{-1}$ is the reference strain rate.

Equation (14) then can be expressed as follows:

$$\dot{D} = aD(1-D)\sigma\frac{\dot{\varepsilon}}{(\dot{\varepsilon}/\dot{\varepsilon}_0)^{\gamma}}, \tag{16}$$

where $a = a_1/b_1$.

The one-dimensional stress-strain relationship without damage can be expressed as

$$\sigma = E\varepsilon, \tag{17}$$

where E, ε are Young's modulus and strain. Considering the effect of damage softening, the stress-strain relationship can be written as

$$\sigma = E\varepsilon(1-D). \tag{18}$$

The differential form of equation (18) is

$$\dot{\sigma} = E(1-D)\dot{\varepsilon} - E\dot{D}\varepsilon. \tag{19}$$

Substitution of equation (16) into equation (19) yields

$$\dot{\sigma} = E(1-D)\dot{\varepsilon}\left[1 - a\left(\frac{\dot{\varepsilon}_0}{\dot{\varepsilon}}\right)^{\gamma} D\sigma\varepsilon\right]. \tag{20}$$

A combination of equations (16) and (20) provides a differential form to describe the constitutive relationship of SFRSCC with damage under uniaxial compression. Two material parameters, a and γ, in the damage evolution model (equation (16)) can be determined by fitting the experimental data. A least square method was used to fit the stress-strain curves of SFRSCC. The optimal parameters a and γ in the damage model for different types of SFRSCC are listed in Table 5.

The stress-strain curves calculated based on the proposed damage model are shown in Figure 10 and compared with the experimental curves. The theoretical curves well illustrated the rate effect on strength of SFRSCC and showed good consistency with the relevant experimental data which indicated that the proposed dynamic damage constitutive model was credible to describe the dynamic stress-strain relationship of SFRSCC under uniaxial compression.

4. Conclusions

The dynamic compression tests of SFRSCC with two strength classes (40 MPa and 60 MPa) were carried out using a 74 mm diameter SHPB. The dynamic compressive stress-strain curves were obtained, and the effects of the matrix strength and fibre content on the strain rate sensitivity of SFRSCC were studied. Following conclusions can be drawn from the present study:

(1) SFRSCC exhibited significant rate sensitivity, whereby the dynamic compressive strength increased with the increase of strain rate. The strain rate sensitivity of SFRSCC was affected by both matrix strength and fibre content. Medium strength SFRSCC showed higher strain rate sensitivity than high strength SFRSCC in the strain rate range of $50\,\mathrm{s}^{-1}$–$240\,\mathrm{s}^{-1}$. The DIF values of medium strength SFRSCC were increased with the increase of fibre content, but for high strength SFRSCC, the DIF values tended to decrease when the fibre content was more than 1.5%. The mix proportion and compaction levels of SFRSCC were considered to be the main factors affecting the strain rate sensitivity.

(2) An empirical formula was proposed to describe the strain rate sensitivity of the SFRSCC by assuming a linear increase in DIF with the logarithm of the strain rate.

(3) A damage constitutive model for SFRSCC was derived based on the equivalent microvoid hypothesis. The theoretical stress-strain curves calculated based on the proposed model could well illustrate the rate effect of SFRSCC and the damage softening process. Due to the few parameters involved, the model can be easily used to evaluate the dynamic compressive behavior of SFRSCC with reasonable accuracy.

Data Availability

The data used to support the findings of this study are available from the corresponding author upon request.

Conflicts of Interest

The authors declare that there are no conflicts of interest regarding the publication of this paper.

Acknowledgments

This research was funded by the National Natural Science Foundation of China (Grant nos. 11502099 and 11802001), for which the authors are grateful.

References

[1] M. Nili and V. Afroughsabet, "Combined effect of silica fume and steel fibers on the impact resistance and mechanical properties of concrete," *International Journal of Impact Engineering*, vol. 37, no. 8, pp. 879–886, 2010.

[2] R. Shao, C. Wu, Y. Su et al., "Experimental and numerical investigations of penetration resistance of ultra-high strength concrete protected with ceramic balls subjected to projectile impact," *Ceramics International*, vol. 45, no. 6, pp. 7961–7975, 2019.

[3] A. N. Dancygier, D. Z. Yankelevsky, and C. Jaegermann, "Response of high performance concrete plates to impact of non-deforming projectiles," *International Journal of Impact Engineering*, vol. 34, no. 11, pp. 1768–1779, 2007.

[4] F. Y. Li, C. Y. Cao, Y. X. Cui, and P. Wu, "Experimental study of the basic mechanical properties of directionally distributed steel fibre-reinforced concrete," *Advances in Materials Science and Engineering*, vol. 2018, Article ID 3578182, 11 pages, 2018.
[5] M. Usman, S. H. Farooq, M. Umair, and A. Hanif, "Axial compressive behavior of confined steel fiber reinforced high strength concrete," *Construction and Building Materials*, vol. 230, 2020.
[6] L. Li, R. Zhang, L. Jin, X. Du, J. Wu, and W. Duan, "Experimental study on dynamic compressive behavior of steel fiber reinforced concrete at elevated temperatures," *Construction and Building Materials*, vol. 210, pp. 673–684, 2019.
[7] K. H. Mo, S. P. Yap, U. J. Alengaram, M. Z. Jumaat, and C. H. Bu, "Impact resistance of hybrid fibre-reinforced oil palm shell concrete," *Construction and Building Materials*, vol. 50, pp. 499–507, 2014.
[8] S. Wang, M.-H. Zhang, and S. T. Quek, "Mechanical behavior of fiber-reinforced high-strength concrete subjected to high strain-rate compressive loading," *Construction and Building Materials*, vol. 31, pp. 1–11, 2012.
[9] V. R. Ramkumar, G. Murali, N. P. Asrani, and K. Karthikeyan, "Development of a novel low carbon cementitious two stage layered fibrous concrete with superior impact strength," *Journal of Building Engineering*, vol. 25, Article ID 100841, 2019.
[10] A. R. Khaloo and M. Afshari, "Flexural behaviour of small steel fibre reinforced concrete slabs," *Cement and Concrete Composites*, vol. 27, no. 1, pp. 141–149, 2005.
[11] A. Baricevic, D. Bjegovic, and M. Skazlic, "Hybrid fiber-reinforced concrete with unsorted recycled-tire steel fibers," *Journal of Materials in Civil Engineering*, vol. 29, no. 6, 2017.
[12] C. C. Hung, Y. T. Chen, and C. H. Yen, "Workability, fiber distribution, and mechanical properties of UHPC with hooked end steel macro-fibers," *Construction and Building Materials*, vol. 260, 2020.
[13] D.-Y. Yoo and N. Banthia, "Mechanical and structural behaviors of ultra-high-performance fiber-reinforced concrete subjected to impact and blast," *Construction and Building Materials*, vol. 149, pp. 416–431, 2017.
[14] S. C. Kou and C. S. Poon, "Properties of self-compacting concrete prepared with coarse and fine recycled concrete aggregates," *Cement and Concrete Composites*, vol. 31, no. 9, pp. 622–627, 2009.
[15] M. Pajak and T. Ponikiewski, "Flexural behavior of self-compacting concrete reinforced with different types of steel fibers," *Construction and Building Materials*, vol. 47, pp. 397–408, 2013.
[16] A. Khaloo, E. Molaei Raisi, P. Hosseini, and H. Tahsiri, "Mechanical performance of self-compacting concrete reinforced with steel fibers," *Construction and Building Materials*, vol. 51, pp. 179–186, 2014.
[17] F. Aslani and S. Nejadi, "Self-compacting concrete incorporating steel and polypropylene fibers: compressive and tensile strengths, moduli of elasticity and rupture, compressive stress-strain curve, and energy dissipated under compression," *Composites Part B: Engineering*, vol. 53, pp. 121–133, 2013.
[18] O. Gencel, W. Brostow, T. Datashvili, and M. Thedford, "Workability and mechanical performance of steel fiber-reinforced self-compacting concrete with fly ash," *Composite Interfaces*, vol. 18, no. 2, pp. 169–184, 2011.
[19] X. Ding, C. Li, B. Han, Y. Lu, and S. Zhao, "Effects of different deformed steel-fibers on preparation and fundamental properties of self-compacting SFRC," *Construction and Building Materials*, vol. 168, pp. 471–481, 2018.
[20] A. H. Nahhab and A. K. Ketab, "Influence of content and maximum size of light expanded clay aggregate on the fresh, strength, and durability properties of self-compacting lightweight concrete reinforced with micro steel fibers," *Construction and Building Materials*, vol. 233, 2020.
[21] M. Ghasemi, M. R. Ghasemi, and S. R. Mousavi, "Investigating the effects of maximum aggregate size on self-compacting steel fiber reinforced concrete fracture parameters," *Construction and Building Materials*, vol. 162, pp. 674–682, 2018.
[22] R. Madandoust, M. M. Ranjbar, R. Ghavidel, and S. Fatemeh Shahabi, "Assessment of factors influencing mechanical properties of steel fiber reinforced self-compacting concrete," *Materials & Design*, vol. 83, pp. 284–294, 2015.
[23] O. Sucharda, P. Lehner, P. Konečný, and T. Ponikiewski, "Investigation of fracture properties by inverse analysis on selected SCC concrete beams with different amount of fibres," *Procedia Structural Integrity*, vol. 13, pp. 1533–1538, 2018.
[24] D. L. Grote, S. W. Park, and M. Zhou, "Dynamic behavior of concrete at high strain rates and pressures: I. experimental characterization," *International Journal of Impact Engineering*, vol. 25, no. 9, pp. 869–886, 2001.
[25] L. J. Malvar and C. A. Ross, "Review of strain rate effects for concrete in tension," *ACI Materials Journal*, vol. 95, no. 6, 1998.
[26] W. Suaris and S. P. Shah, "Strain-rate effects in fibre-reinforced concrete subjected to impact and impulsive loading," *Composites*, vol. 13, no. 2, pp. 153–159, 1982.
[27] G. Ruiz, A. de la Rosa, L. C. Almeida et al., "Dynamic mixed-mode fracture in SCC reinforced with steel fibers: an experimental study," *International Journal of Impact Engineering*, vol. 129, pp. 101–111, 2019.
[28] M. Pajak, J. Janiszewski, and L. Kruszka, "Laboratory investigation on the influence of high compressive strain rates on the hybrid fibre reinforced self-compacting concrete," *Construction and Building Materials*, vol. 227, 2019.
[29] E. Kantar, T. Y. P. Yuen, V. Kobya, and J. S. Kuang, "Impact dynamics and energy dissipation capacity of fibre-reinforced self-compacting concrete plates," *Construction and Building Materials*, vol. 138, pp. 383–397, 2017.
[30] S. R. Abid, M. L. Abdul-Hussein, N. S. Ayoob, S. H. Ali, and A. L. Kadhum, "Repeated drop-weight impact tests on self-compacting concrete reinforced with micro-steel fiber," *Heliyon*, vol. 6, no. 1, Article ID e03198, 2020.
[31] N. Li, Z. Q. Jin, G. C. Long et al., "Impact resistance of steel fiber-reinforced self-compacting concrete (SCC) at high strain rates," *Journal of Building Engineering*, vol. 38, 2021.
[32] N. Burlion, F. Gatuingt, G. Pijaudier-Cabot, and L. Daudeville, "Compaction and tensile damage in concrete: constitutive modelling and application to dynamics," *Computer Methods in Applied Mechanics and Engineering*, vol. 183, no. 3-4, pp. 291–308, 2000.
[33] T. J. Holmquist, G. R. Johnson, and W. H. Cook, "A computational constitutive model for concrete subjected to large strains,high strain rates, and high pressures," in *Proceedings of the 14th International Symposium on Ballistics*, pp. 591–600, Quebec, Canada, 1993.
[34] R. Y. Huang, Y. C. Li, J. Zhang, and G. Gao, "Application of damage evolution equation under coupled compression-shear to constitutive model of concrete," *Transactions of Beijing Institute of Technology*, vol. 33, no. 6, pp. 551–555, 2013.
[35] EFNARC, *The European Guidelines for Self-Compacting Concrete, Specification, Production and Use*, The European Federation of Specialist Construction Chemicals and Concrete Systems, Farnham, UK, 2005.

[36] H. Kolsky, "An investigation of the mechanical properties of materials at very high rates of loading," *Proceedings of the Physical Society Section B*, vol. 62, no. 11, pp. 676–700, 1949.

[37] M. Hassan and K. Wille, "Comparative experimental investigations on the compressive impact behavior of fiber-reinforced ultra high-performance concretes using split Hopkinson pressure bar," *Construction and Building Materials*, vol. 191, pp. 398–410, 2018.

[38] FIB, *Fib Model Code for Concrete Structure 2010*, Ernst & Sohn, Berlin, Germany, 2013.